PCCP

Accepted Manuscript

ROYAL SOCIETY OF CHEMISTRY

www.rsc.org/pccp

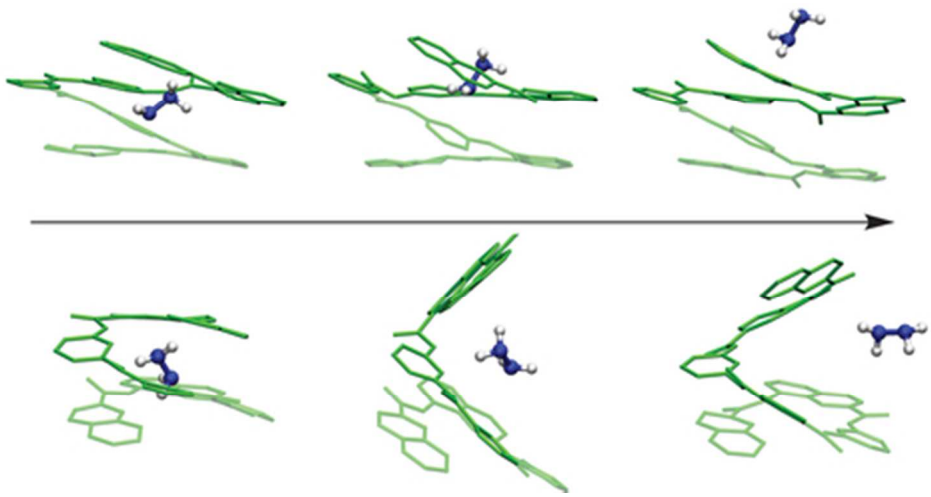

A hydrazine molecule encapsulated in an arylamide helical foldamer escaping from the "top" (top) and "side" (bottom) of the capsule in the aqueous and methanol solution, respectively.
39x20mm (300 x 300 DPI)

Cite this: DOI: 10.1039/c0xx00000x

www.rsc.org/xxxxxx

COMMUNICATION

Mechanistic and Dynamic Insights into Ligand Encapsulation by Helical Arylamide Foldamers

Ara M. Abramyan,[a] Zhiwei Liu,[a] Vojislava Pophristic *[a]

Received (in XXX, XXX) Xth XXXXXXXXX 20XX, Accepted Xth XXXXXXXXX 20XX

DOI: 10.1039/b000000x

Molecular capsules have been extensively used in catalysis, drug delivery, molecular recognition and protection of ligands from degradation. Novel "apple peel" shaped helical arylamide capsules have been experimentally pursued due to their flexible nature and designability. They were found to encapsulate a variety of small molecules. The apple peel shape of the capsules led to a hypothesis that binding and release of ligands involve partial unfolding. However, the exact mechanism is unknown. Using molecular dynamics simulations with our new aryl-amide force field parameters, we identify two low energy barrier binding/release mechanisms, in which the capsule helical structure is either minimally disturbed or restored quickly (within 100 ps). Furthermore, we determine the effects of ligand sizes, their chemical nature (hydrogen bonding capabilities), and solvents on binding modes and stabilities. Our findings not only support experimental observations but also provide underlying principles that allow for rational design of foldamer capsules.

Encapsulation enables isolation of molecules from their environment, often used in strengthening molecular recognition,[1] catalysis,[2] drug delivery[3] and protection of guest species from degradation.[4] Helical capsules[5–9] based on arylamide foldamers[10–12] are of particular interest due to their flexible nature and structural features that facilitate rational design. Their advantage over rigid capsules[13,14] has been demonstrated by "apple peel" shaped arylamide helices[5,6] with hybrid sequences (e.g. oligoamide **O1** in Figure 1). X-ray and NMR experiments have confirmed the presence of ligands inside these capsules as well as exchange between bound and free guests.[5,6,8] In particular, the X-ray structure of a capsule-water complex implies that the bound ligand interacts with the capsule via hydrogen bonds (H-bonds).[5] Due to the highly curved terminal quinoline units, the radius of the helix becomes smaller towards the termini to close off the capsule. Therefore, it is speculated that partial unfolding of the helix is necessary for the binding and release of the guest molecule.[5,6,8] However, no detailed information on ligand-capsule interactions and dynamics or on the mechanism of encapsulation has been reported, despite the fact that such information is crucial for rational design of capsules. In this paper, we present a computationally derived mechanism of ligand encapsulation by helical oligoamide.

In recent years, we have focused on developing a strategy[15–17] that allows for accurate prediction of arylamide foldamer structures. Using the optimized aryl-amide torsional parameters we conducted all-atom molecular dynamics (MD) simulations of helical arylamide capsules **O1** (Figure 1), **O2** and **O3**, with hybrid pyridine-quinoline sequences differing only in the number of pyridine units (3, 5, and 7, respectively). Binding of five ligands with each capsule was studied. The ligands are: water (H_2O), hydrogen peroxide (H_2O_2), hydrazine (N_2H_4), formic acid (HCOOH) and methanol (CH_3OH). To examine the influence of environment, we used three explicit solvents with varying polarity and H-bonding capabilities - water, methanol and chloroform. Every simulation box measured ~50-60 Å along each side and contained one capsule-ligand complex and up to ~3500 solvent molecules. The NVT production runs were 50 ns each following NPT equilibrations (~500 ps) at 300K and 1 atm. The initial **O1**-ligand structure was constructed by placing the ligand, randomly orientated, in the centre of a pre-equilibrated capsule. For selected systems, additional simulations (details in Table S1) from different **O1**-ligand initial structures were carried out.

Being that **O1** is the smallest and least favourably binds larger ligands, it allowed the simulation to capture ligand release under ambient conditions within reasonable time scale. This in turn provided a basis for a systematic comparison for a range of ligands and solvents, to assess capsule-ligand interactions, conformations and stabilities, as well as binding/release mechanism. Our results explain and add to experimental findings.

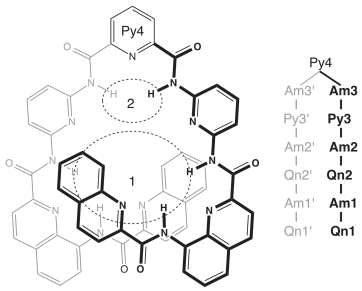

Figure 1. Structure, numbering and schematic of the two binding sites of the oligoamide capsule **O1**.

Analysis of the MD trajectories reveals that the **O1**-ligand interactions, as expected, heavily rely on H-bonding. Based on H-bonding patterns and proximity, we identified two binding sites

within the central cavity of **O1** (Figure 1). Site 1 is characterized by ligand interactions with surrounding quinolines Qn1(1'), Qn2(2') and amides Am1(1'), Am2(2'). In site 2, ligand interacts with Am3(3'). Py3(3') pyridines are located between sites 1 and 2. The sites are not mutually exclusive - the larger ligands interact with both sites simultaneously.

In all solvents, H_2O resides in site 1 (Figure 2a). The O_{water} (O_w) atom H-bonds with Am2(2') and Am1(1') 85-90% and 40-50% of the time, respectively. H_2O rotates around its C2 axis on a 10 ps scale. As a result, the H_2O plane alternates between two positions: a) aligned with the helical axis (vertical to the Py4 plane), forming two H-bonds (one for each H_w) with $N_{aromatic}$ (N_a) of Qn1(1'); and b) horizontal to the Py4 plane, forming two H_w---N_a (Py3(3')) H-bonds. Interestingly, the polarity of the solvent affects the vertical/horizontal ratio of H_2O binding (70/30 in chloroform, 62/38 in methanol, 54/46 in water).

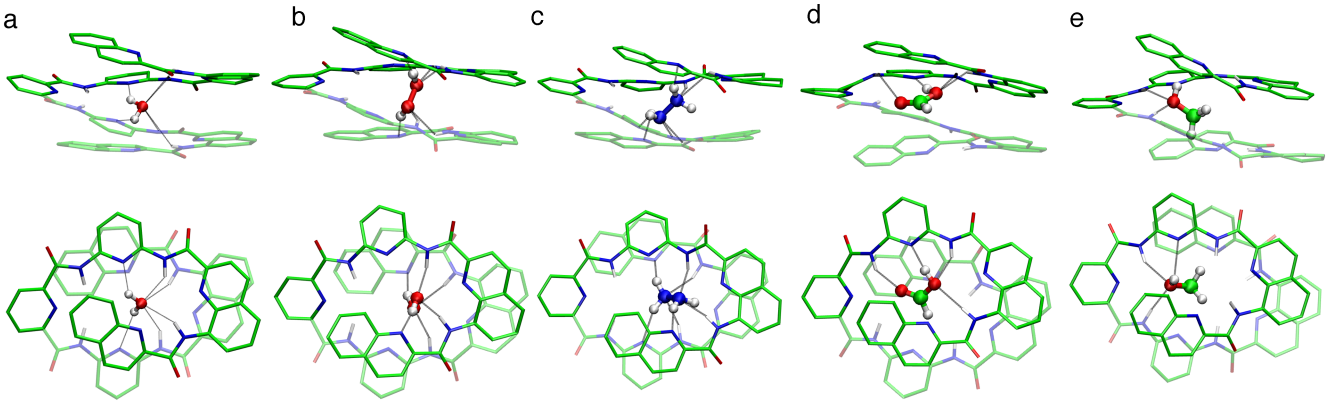

Figure 2. The **O1**-ligand complexes showing the major binding mode (side and top views). The ligands are H_2O (a), H_2O_2 (b), N_2H_4 (c), HCOOH (d) and CH_3OH (e).

The X-ray structure[5] of the **O1**-H_2O complex shows, however, that O_w is in position corresponding to site 2 rather than site 1. We therefore performed two independent simulations: one starting from the X-ray structure, and the other with H_2O randomly placed inside the cavity. Both simulations converged to the binding mode discussed above. The difference between X-ray and MD binding modes can be attributed to the MD simulation conditions being dynamic rather than static. In addition, the MD observed binding mode has more H-bonds, which is energetically more favourable.

H_2O_2 adopts a *trans* configuration and resides in site 1 most of the time. In the major binding mode, H_2O_2 is oriented so that its O-O bond roughly aligns with the helical axis of **O1** (Figure 2b). One $O_{peroxide}$ (O_p) atom H-bonds with Am1/Am2 and the other O_p interacts with Am1'/Am2'. The $H_{peroxide}$ atoms H-bond with the N_a atoms in Qn1(1'). The two OH groups exchange positions by rotating around the molecule's C2 axis, with the residence time of <500 ps for each position. During the rotation, the molecule lingers at a roughly horizontal (with respect to the Py4 plane) position in which one O_p remains in site 1, whereas the other intrudes into site 2 and interacts with the Am3(3'). Similarly to H_2O, H_2O_2's tendency for binding in horizontal position increases with the solvent polarity, from 15% in chloroform, to 19% and 24% in methanol and water, respectively.

N_2H_4 behaves similarly to H_2O_2. In the major binding mode, one of the $N_{hydrazine}$(N_h) atoms interacts with Am1/Am2, while the other one H-bonds with Am1'/Am2' (Figure 2c). N_2H_4 also rotates around its C2 axis with the exchange rate of ~400 ps. The H_h atoms form H-bonds with the N_a atoms of Qn1(1'), Qn2(2') and Py3(3') whenever they are brought into proximity by the rotation. N_2H_4 however remains in the horizontal position less of the time (<5%) than H_2O_2. The difference is likely due to stronger H-bonds between O_p and protons of Am3(3') in the **O1**-H_2O_2 complex.

The binding of HCOOH differs from the three ligands discussed above. The simulation shows that HCOOH lies in the Py4 plane (Figure 2d) and forms H-bond with both site 1 and 2 groups. We observed two binding modes characterized by rotation around the C-H bond. In binding mode I, $O_{carbonyl}$ (O_c) is in site 2 and H-bonded to the Am3(3') protons whereas $O_{hydroxyl}$ (O_h) is in site 1 interacting with Am2/Am1 or Am2'/Am1'. The flipping between Am2/Am1 and Am2'/Am1' capsule cones is a result of the rotation around the C=O bond on the scale of ~100 ps. In binding mode II, O_h is H-bonded to Am3(3'), whereas O_c interacts with either Am2/Am1 or Am2'/Am1'. In both binding modes I and II, $H_{hydroxyl}$ forms H-bonds with N_a atoms in Py3(3'), and occasionally with those in Qn1(1'). The exchange between binding modes I and II is slow, occurring twice in 50 ns (chloroform), once in 3.1 ns (methanol) and zero times in 2.7 ns (water). The low number of observed exchanges between modes indicates that enhanced sampling methods are needed for the determination of a major binding mode.

The binding of CH_3OH is also bimodal: its O atom H-bonds to amides in site 1 or 2 (Figure 2e). The exchange between these two modes occurs on average every ~150 ps. Compared to other ligands, CH_3OH leaves **O1** early on in all three solvents (Table 1). Additional simulations (Table S1) starting from bound configurations extracted from previous runs and with re-initialized velocities result in similarly short encapsulation durations. This is due to weaker ligand-capsule interaction (i.e. only one H-bonding group in CH_3OH), and CH_3OH's relatively bulky methyl group which sterically interferes with **O1**, opening it up for the ligand to leave. Our MD data shows that CH_3OH mostly resides in site 1 in water, site 2 in methanol, and both sites 1 and 2 (50/50) in chloroform. However, the total residence times in specific sites for both water (~300 ps) and methanol (~400 ps) are too short to determine whether this solvent-dependent preference is reliable.

Next, we analyze **O1** conformational changes upon ligand binding in terms of foldamer backbone curvature and pitch, which measure capsule distortions in the planes perpendicular and parallel to the helical axis, respectively. The curvature angle is defined by the centers of mass (COMs) of three consecutive aromatic rings. There are five curvature angles, three of which are unique due to symmetry: Qn1-Qn2-Py3/Qn1'-Qn2'-Py3' (∠1), Qn2-Py3-Py4/Qn2'-Py3'-Py4 (∠2) and Py3-Py4-Py3' (central angle, ∠c). Upon ligand binding, ∠c increases in the order of H_2O, N_2H_4, H_2O_2, CH_3OH, HCOOH by up to 10° (Figure 3a), whereas ∠1 and ∠2 increase to a lesser extent (<5°). The order correlates well with ligand size and in the following cases is affected by binding location: the stronger binding interaction between H_2O_2 (or HCOOH) and site 1 leads to larger shift of the ∠c distribution (Figure 3a) than that of N_2H_4 (or CH_3OH). The fact that the most significant change of the capsule curvature upon binding of all ligands (except H_2O) occurs at the capsule's central hollow, rather than the cone-like parts, points to the importance of the flexibility of central backbone part in capsule design.

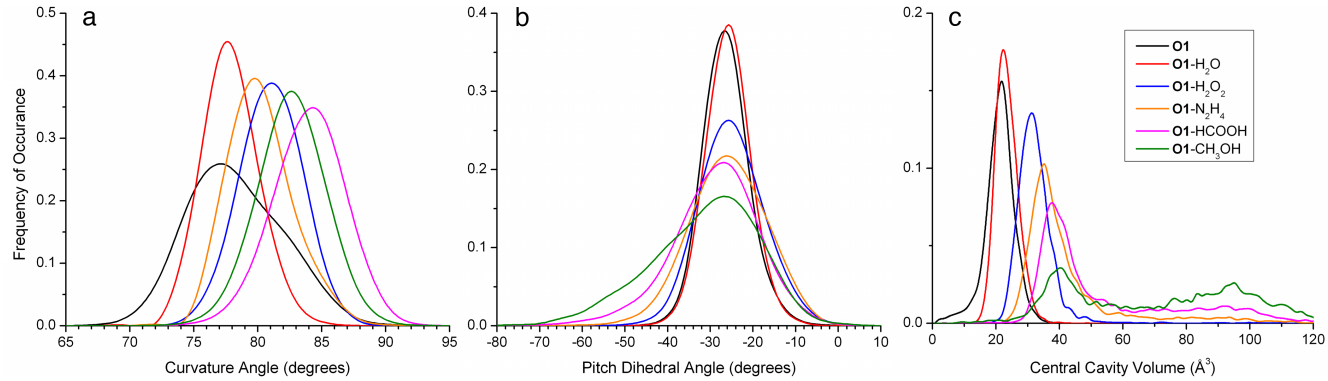

Figure 3. Distributions of (a) the central curvature angle ∠c, (b) the pitch dihedral angle ∠Qn1-Qn2-Py3-Py4, and (c) the central cavity volume of **O1** in chloroform, based on up to 50 ns MD trajectory of **O1** and bound **O1**-ligand systems.

The **O1** helical pitch is measured as the dihedral angle defined by the COMs of four consecutive aromatic rings. Figure 3b shows an example of the pitch dihedral angle distribution (Qn1-Qn2-Py3-Py4) for **O1** and **O1**-ligand complexes. Except for H_2O, all ligands broaden the pitch dihedral angle distribution as **O1** "breathes" more actively when a ligand is encapsulated. The pitch dihedral angle distribution width (and hence the capsule distortion along its helical axis) increases in the order of H_2O, H_2O_2, N_2H_4, HCOOH, CH_3OH. The curvature and pitch changes upon ligand binding are similar in all three solvents.

Also shown in Figure 3c is the distribution of the central cavity volumes (main peaks at < 60 Å^3), ranging from ~20Å^3 to ~40Å^3 and increasing when necessary to accommodate ligands of larger sizes.[18] The increase in the central cavity volume correlates very well with the conformational distortions, especially with the pitch dihedral angle distributions. The relatively small changes in capsule's geometry (curvature, pitch) resulting in significant changes in cavity volumes clearly demonstrate the flexibility of foldamer capsules.

The levels of **O1** conformational distortion correlate inversely with the duration of ligand encapsulation (Table 1). Although the difference in time scales prevents a direct comparison of our simulation (50 ns) with solution NMR results,[6] the trend and the binding data are in general consistent with experimental findings that H_2O binds most favorably, followed by H_2O_2 and N_2H_4, then by HCOOH and CH_3OH.[6] Therefore, the duration of ligand encapsulation is used here to gauge the stabilities of **O1**-ligand complexes. Table 1 indicates that ligand sizes, H-bonding capability, and solvent properties all play a role in the stabilities of **O1**-ligand binding. The smallest ligands (H_2O and H_2O_2) form the most stable **O1**-ligand complexes and remain encapsulated the longest. CH_3OH, the largest ligand with the least H-bonding sites, departs from **O1** most rapidly. N_2H_4 and HCOOH don't follow a clear trend because of the competing size and H-bonding factors: N_2H_4 is smaller than HCOOH, whereas HCOOH has better H-bonding capability than N_2H_4. In addition, the duration of ligand encapsulation decreases as the polarity (and H-bonding capability) of the solvent increases. This can be attributed to the observed capsule-solvent H-bonding interactions in polar protic solvents that increase the conformational fluctuations of **O1**.[19,20]

Table 1. Release mechanisms and timings of ligand departure.

	water	methanol[a]	chloroform[a]
H_2O	Top, ~25ns	x	x
H_2O_2	Top, ~6.2ns	Top, ~6.3ns	x
N_2H_4	Top, ~1ns	Side, ~6.4ns	Top, ~38.8ns
HCOOH	Top, ~2.7ns	Side, ~3.1ns	x
CH_3OH	Top, ~0.3ns	Side, ~0.4ns	Side, ~12ns

[a] x indicates cases where ligands did not leave within 50 ns.

By analyzing the conformational changes around the time of ligand departure, we can provide insight into ligand binding/release mechanism. We identified two types of ligand release mechanisms: sliding out from the "top" (Figure 4a) and leaving upon a "side" opening (Figure 4b) of **O1**. The "top" mechanism does not require major conformational deformation of **O1**. This suggests that **O1** does not need to unfold to allow the binding or release of ligand. On the other hand, the "side" release requires significant deformation of **O1** (Figure 4b). Since the conformation of **O1** is largely determined by the rotations around the aryl-amide ($C_{aromatic}$-$C_{peptide}$ or $C_{aromatic}$-$N_{peptide}$) bonds, we examined the aryl-amide torsional angles around the time of ligand departure, and found no deviation from the normal distribution range. Therefore, the "side" opening of the capsule is

a result of a net effect of small changes (within the normal distribution range) in several torsional angles. Regardless of the ligand release mechanism, the capsule restores the helical structure within 100 ps. These results suggest that: (1) a ligand can enter the capsule the same way it departs; (2) the ligand binding and release are low energy barrier processes.

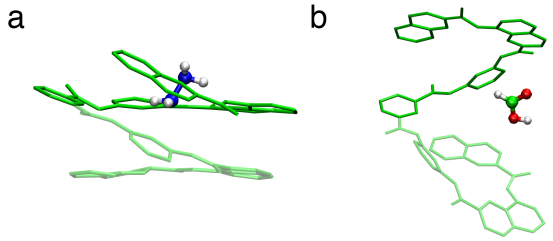

Figure 4. The "top" and "side" mechanisms of ligand departure: (a) N_2H_4 (in chloroform), and (b) HCOOH (in methanol).

The ligand size and its binding positions affect the binding/release mechanism. We observe the following: 1) smaller ligands tend to leave from "top" without significantly distorting the capsule; 2) ligands in site 1 leave from "top" whereas ligands in site 2 leave by a "side" opening. Solvent also plays an important role in binding/release mechanisms. For example, in the aqueous environment the "top" mechanism is exclusive. This is caused by the interaction of water with the capsule backbone and/or parts of encapsulated ligands. Our analysis shows a significant presence (~50-65% of the time) of H-bonds between solvent H_{water} (H_w) and the N_a atoms of Qn1(1'). Furthermore, H_w sometimes H-bonds with ligands through the small opening along the helical axis ("top"). These facts, combined with the observation that all ligands (including HCOOH and CH_3OH) reside primarily in site 1 in the aqueous solution, explains the exclusivity of the "top" mechanism in water. Another example of solvent effect would be N_2H_4 – it leaves from the "side" in methanol and "top" in chloroform. Detailed analysis shows that a solvent molecule approaching from the "side" of **O1** and H-bonding with N_h is responsible for the "side" opening and release of N_2H_4 in methanol.

In conclusion, we found two new low energy barrier binding/release mechanisms. Polarities and H-bonding capabilities of solvents not only influence binding interactions but also affect, sometimes dictate, the binding/release mechanism. In addition, both ligand sizes and H-bonding abilities play vital roles in the binding and stabilities of the **O1**-ligand complexes. The specificity of the host-guest interactions is driven by the relative locations of their H-bond donors and acceptors. The capsule-ligand complexes are highly dynamic, with sub-ns exchange between binding modes. Our results suggest that the binding and release of ligands are thermodynamically governed processes. Notably, regardless of binding positions, the capsule conformational distortion upon ligand binding is highest in its central part indicating possible design direction. This study demonstrates the feasibility of using MD simulations with the proper torsional parameters for providing insight into both the structure and dynamics of arylamide foldamers and their interactions with ligands. Although **O1** is of little practical use due to its small cavity, the **O1**-ligand interactions, dynamics and conformational distortions are similar to those of larger capsules, indicating analogous binding/release mechanisms. To confirm and extend (to larger capsules) our conclusions, we plan to utilize an enhanced sampling method which will provide free energy profiles of the binding/release processes. In addition, we are investigating a variety of new foldamer capsules constructed based on design principles derived from our findings.

Acknowledgement

This research was supported by the NSF MSN-1049771 and MRI CHE-1229564 grants.

Notes and references

[a] *Department of Chemistry & Biochemistry, University of the Sciences, Philadelphia, PA 19104. Fax: 215 596 8543; Tel 215 596 8551; E-mail: v.pophri@usciences.edu*

† Electronic Supplementary Information (ESI) available: Details of molecular dynamics simulation setups and analysis. See DOI: 10.1039/b000000x/

‡ Footnotes should appear here. These might include comments relevant to but not central to the matter under discussion, limited experimental and spectral data, and crystallographic data.

1. M. D. Pluth, D. Fiedler, J. S. Mugridge, R. G. Bergman, and K. N. Raymond, *Proc. Natl. Acad. Sci. U. S. A.*, 2009, **106**, 10438–43.
2. J. Kang and J. Rebek, *Nature*, 1997, **385**, 50–2.
3. D. Ma, G. Hettiarachchi, D. Nguyen, B. Zhang, J. B. Wittenberg, P. Y. Zavalij, V. Briken, and L. Isaacs, *Nature Chem.*, 2012, **4**, 503–10.
4. M. Yoshizawa, T. Kusukawa, M. Fujita, and K. Yamaguchi, *J. Am. Chem. Soc.*, 2000, **122**, 6311–6312.
5. J. Garric, J.-M. Léger, and I. Huc, *Angew. Chem. Int. Ed.*, 2005, **44**, 1954–8.
6. J. Garric, J.-M. Léger, and I. Huc, *Chem. Eur. J.*, 2007, **13**, 8454–62.
7. C. Bao, Q. Gan, B. Kauffmann, H. Jiang, and I. Huc, *Chem. Eur. J.*, 2009, **15**, 11530–6.
8. Y. Ferrand, N. Chandramouli, A. M. Kendhale, C. Aube, B. Kauffmann, A. Grélard, M. Laguerre, D. Dubreuil, and I. Huc, *J. Am. Chem. Soc.*, 2012, **134**, 11282–8.
9. G. Lautrette, C. Aube, Y. Ferrand, M. Pipelier, V. Blot, C. Thobie, B. Kauffmann, D. Dubreuil, and I. Huc, *Chem. Eur. J.*, 2014, **20**, 1547–53.
10. S. H. Gellman, *Acc. Chem. Res.*, 1998, **31**, 173–180.
11. C. M. Goodman, S. Choi, S. Shandler, and W. F. DeGrado, *Nat. Chem. Biol.*, 2007, **3**, 252–62.
12. D.-W. Zhang, X. Zhao, J.-L. Hou, and Z.-T. Li, *Chem. Rev.*, 2012, **112**, 5271–316.
13. L. Kovbasyuk and R. Krämer, *Chem. Rev.*, 2004, **104**, 3161–87.
14. G. W. Gokel, W. M. Leevy, and M. E. Weber, *Chem. Rev.*, 2004, **104**, 2723–50.
15. Z. Liu, A. Teslja, and V. Pophristic, *J. Comput. Chem.*, 2011, **32**, 1846–58.
16. V. Pophristic, S. Vemparala, I. Ivanov, Z. Liu, M. L. Klein, and W. F. DeGrado, *J. Phys. Chem. B*, 2006, **110**, 3517–26.
17. J. F. Galan, J. Brown, J. L. Wildin, Z. Liu, D. Liu, G. Moyna, and V. Pophristic, *J. Phys. Chem. B*, 2009, **113**, 12809–15.
18. R. A. Laskowski, *J. Mol. Graph.*, 1995, **13**, 323–330.
19. Z. Liu, R. C. Remsing, D. Liu, G. Moyna, and V. Pophristic, *J. Phys. Chem. B*, 2009, **113**, 7041–4.
20. J. F. Galan, C. N. Tang, S. Chakrabarty, Z. Liu, G. Moyna, and V. Pophristic, *Phys. Chem. Chem. Phys.*, 2013, **15**, 11883–92.